FISAPS Workshop on Research Using High Vertical-Resolution Radiosonde Data

# Recent research progress based on the measurements of high-resolution radiosonde network in China and the Beijing MST radar observations

Yufang Tian[1], Jianping Guo[2*], Jian Zhang[3], Yanmin Lv[2], Yuping Sun[2], Ze Chen[1]

[1]Institute of Atmospheric Physics, Chinese Academy of Sciences

[2]Chinese Academy of Meteorological Sciences

[3]China University of Geosciences

Jianping Guo (jpguocams@gmail.com)
Yufang Tian (tianyufang@mail.iap.ac.cn)

# High-resolution radiosondes in China

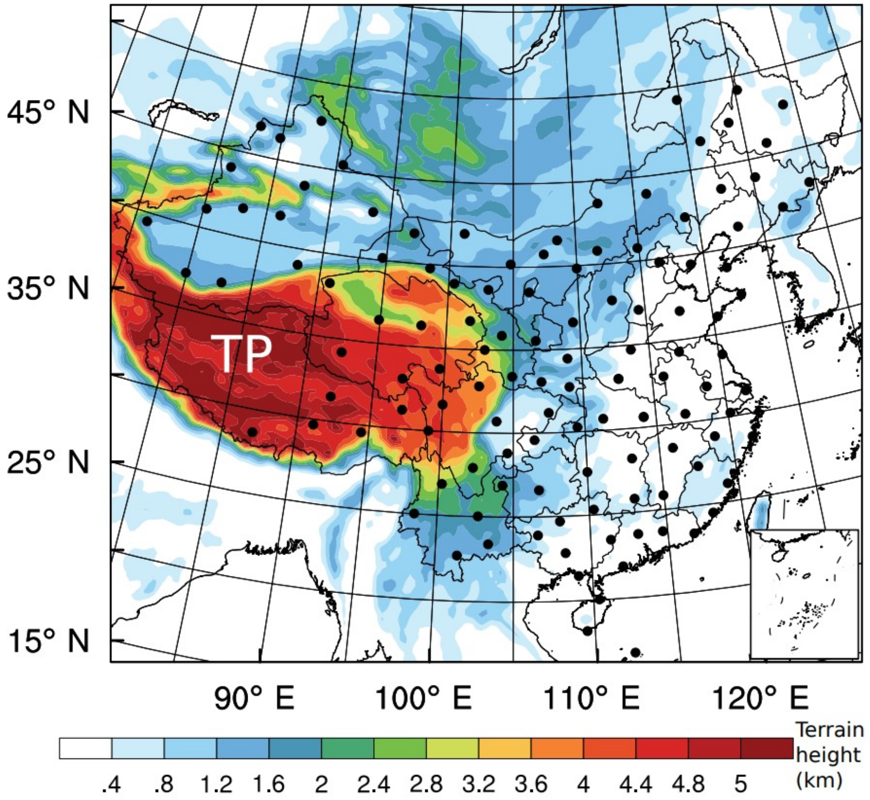


Spatial distribution of CMA sounding sites (black dots), overlaid over the terrain height (color shaded) of China

**2011, 120 operational radiosonde stations using the L-band sounding systems.**

**The GTS1 digital electronic radiosonde**

1 January 2011 to 31 July 2015

| Time | Profiles |
|---|---|
| 02:00 BJT (summer) | 1578 |
| 08:00 BJT | 190 027 |
| 06:00 BJT (summer) | 10 313 |
| 20:00 BJT | 189 634 |
| total | 391 552 |

# BLH derived from high-resolution radiosondes: Climatological pattern

- **The boundary layer height (BLH) is extracted by the bulk Richardson number (Ri) method.**
  (Vogelezang and Holtslag, 1996; Seidel et al. 2012)

$$Ri(z) = \frac{(g/\theta_{vs})(\theta_{vz} - \theta_{vs})(z - z_s)}{(u_z - u_s)^2 + (v_z - u_s)^2 + (bu_*^2)}$$

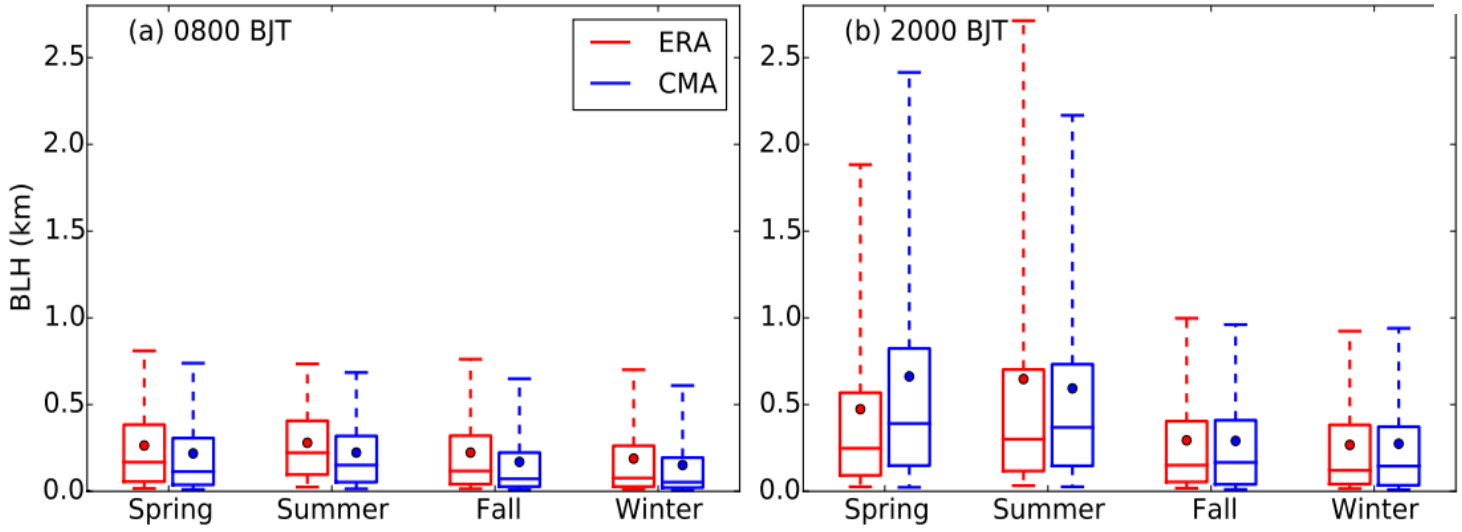


**The BLH of spring and summer is generally higher.**

**At 08:00 BJT, the mean value (dot) of ERA-BLH>CMA-BLH**

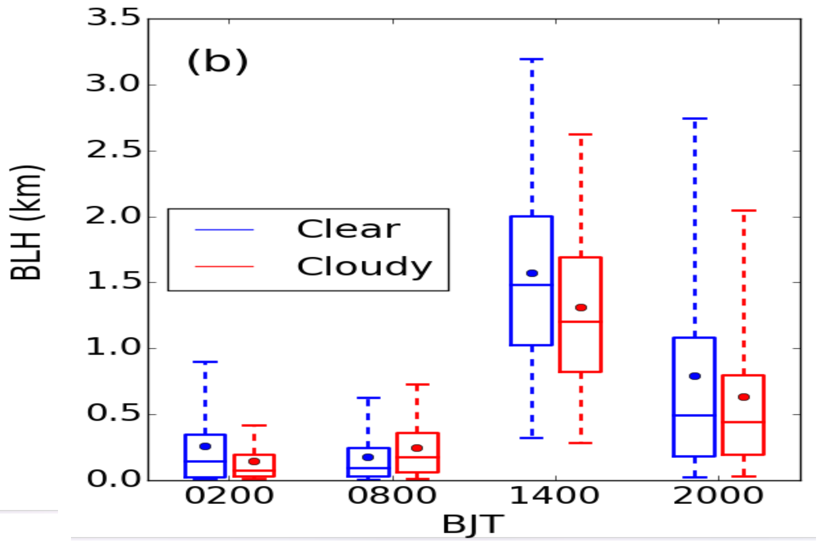


**At 14:00 BJT, the development of PBL is typically suppressed due to less solar radiation received at the surface under cloudy conditions.**

**At 20:00 and 02:00 BJT, higher BLHs under clear conditions, my be related to the larger heat storage of land surface.**

Guo et al. Atmos Chem Phys 2016

# BLH derived from high-resolution radiosondes: Climatological pattern

- The BLH presents the opposite gradient spatial distribution at 08:00 and 20:00 BJT
- These are likely caused by the differing magnitudes of solar radiation in the west (at an earlier local sidereal time) and east of China.

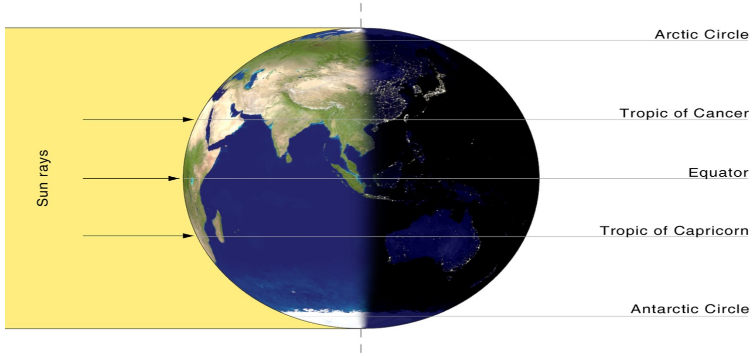


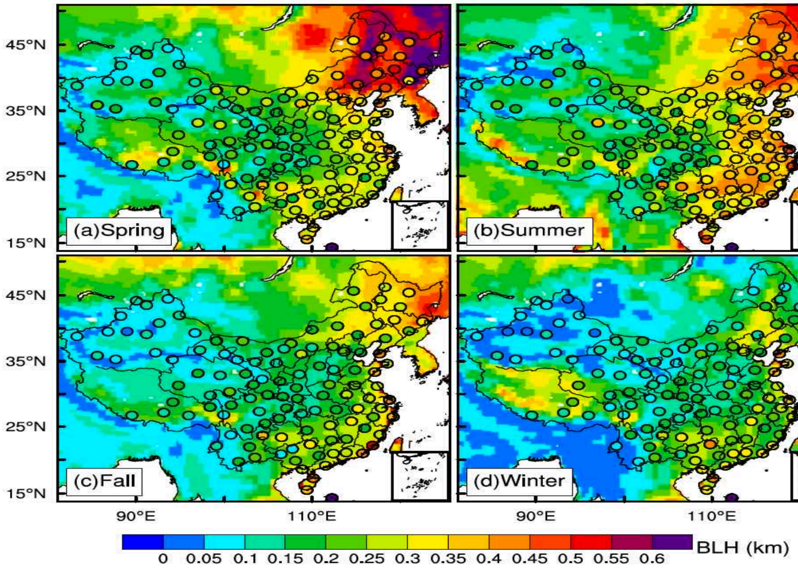


PBL height at 0800 BJT

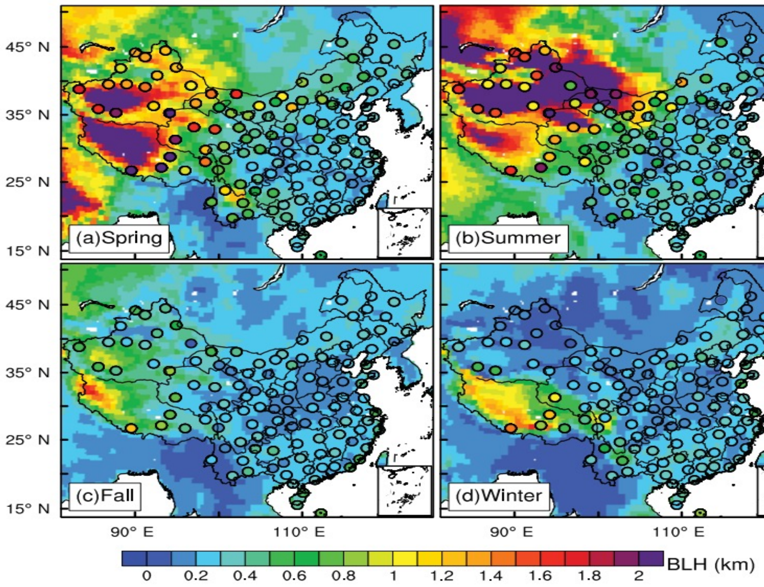


PBL height at 2000 BJT

Guo et al. Atmos Chem Phys 2016

# BLH derived from high-resolution radiosondes: Climatological pattern

- Data: Intensive summertime soundings launched **at 1400 BJT** (2012~2016)
- Method: The PBL with different thermodynamic stability were determined by calculating the near-surface potential temperature difference (PTD) .
- **A prominent north–south gradient** with higher BLH in northwest China.

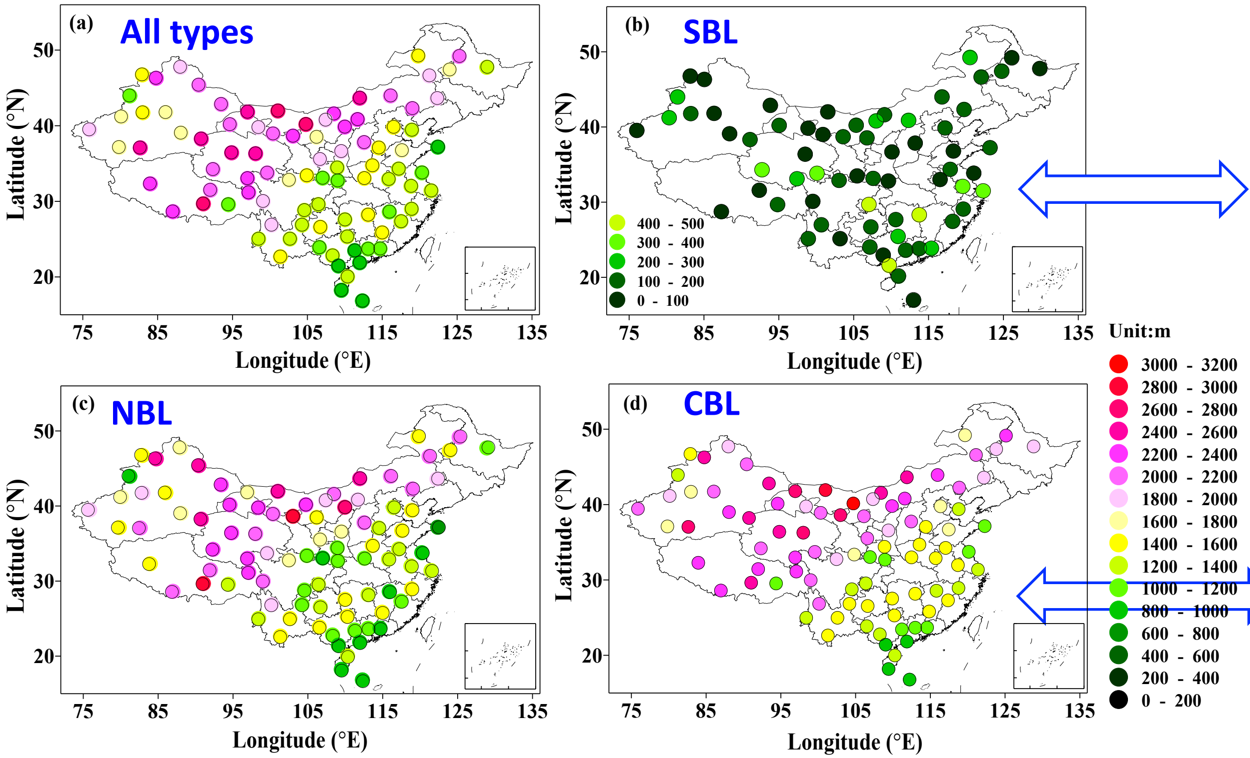


Cloud cover

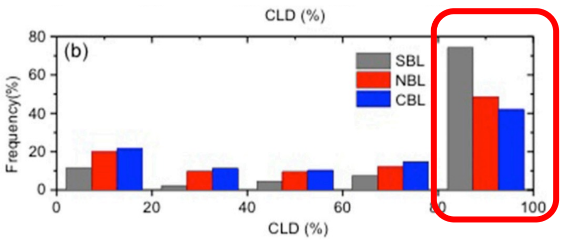


Sensible heat flux

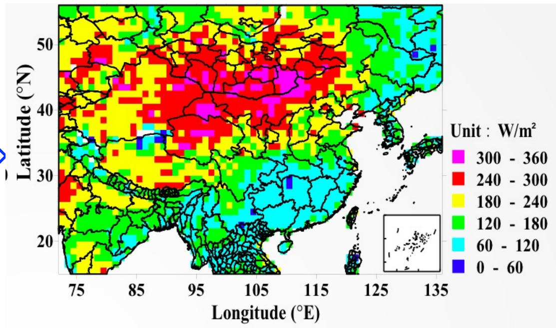


- The evolution of SBL height is mainly determined by cloud cover.
- CBL height is mainly determined by the observation of sensible heat flux.

Zhang & Guo* et al. J. Climate 2018

# BLH derived from high-resolution radiosondes: Meteorological influence

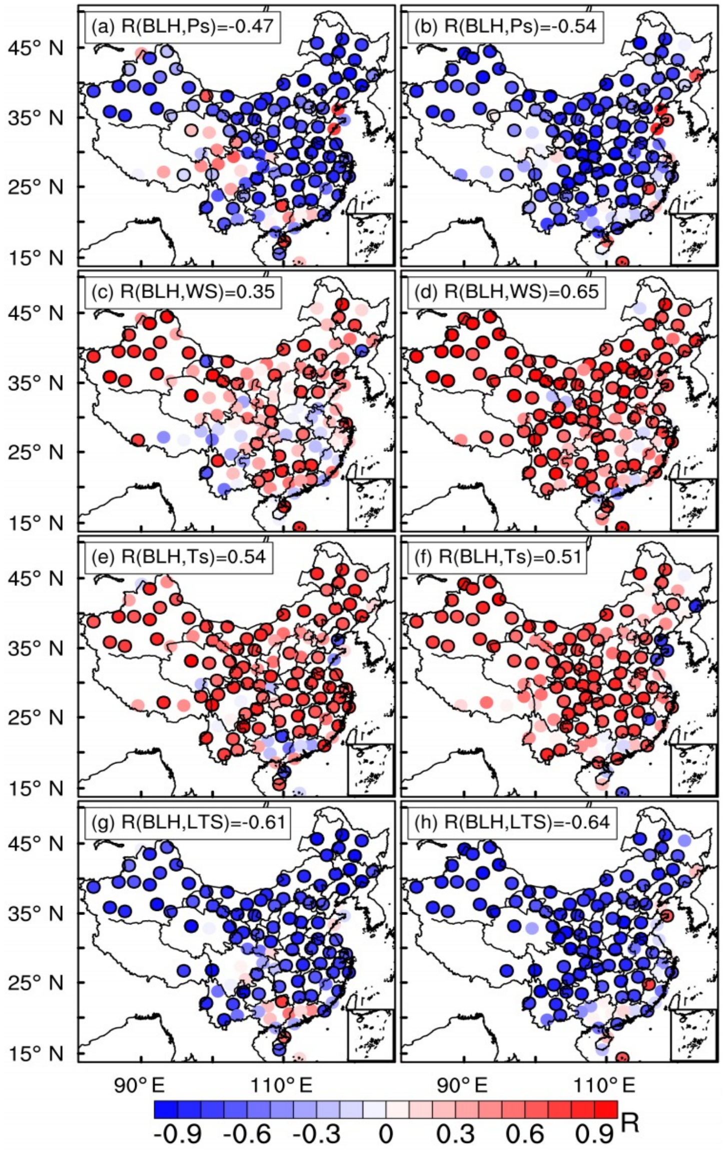


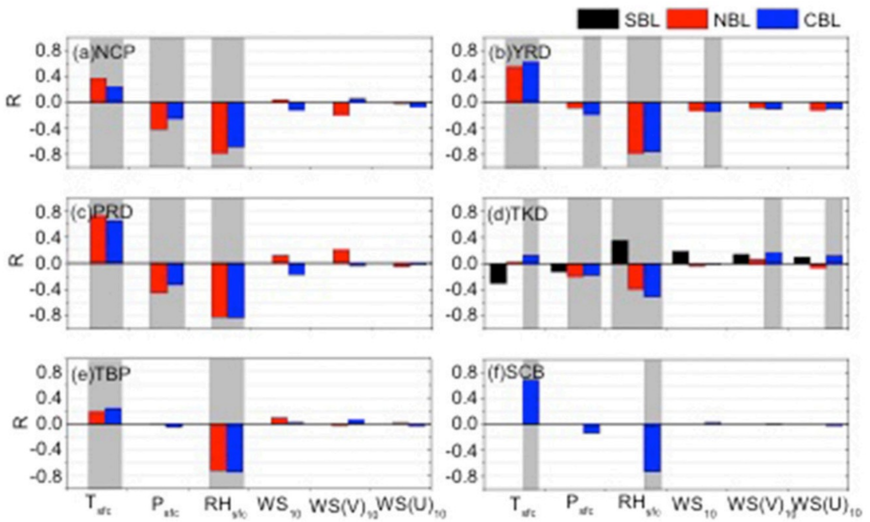


- This annual cycle of BLH at most sites is found to be anti -correlated with the surface pressure, lower tropospheric stability (LTS), and humidity (CBL,NBL).
- And positively correlated with the near-surface wind speed and temperature (CBL,NBL), whereas no apparent relationship was found for SBL.



Guo et al. Atmos Chem Phys 2016 Zhang & Guo* et al. J. Climate 2018

# BLH trend derived from radiosondes @14 BJT

- Long-term change trend of BLH in China (1979-2016) is reversed in the year of 2004
- BLH increased uniformly at first and  decreased inhomogeneously over the latter period

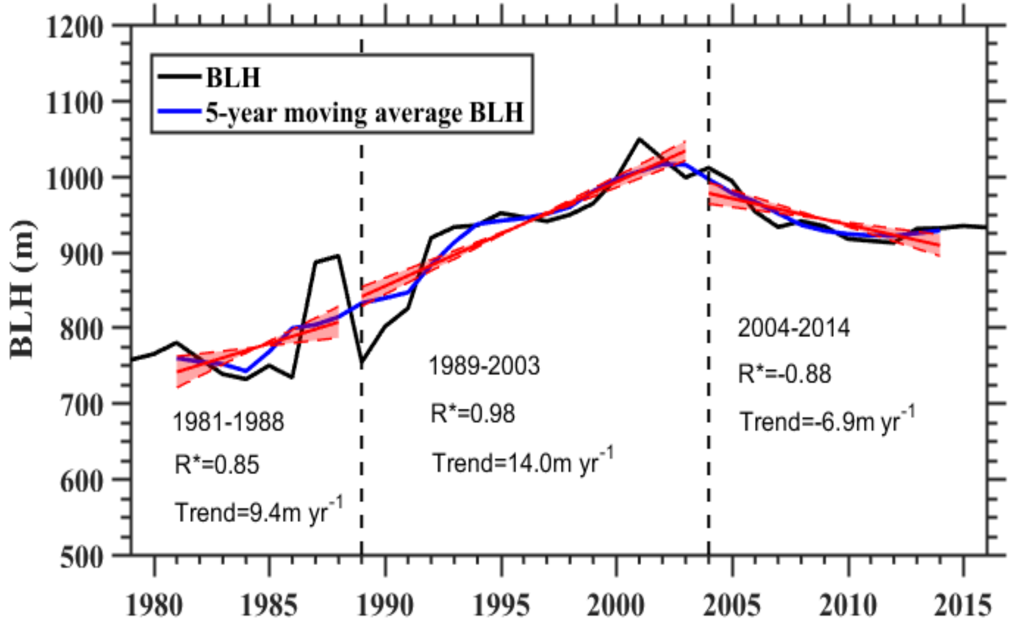


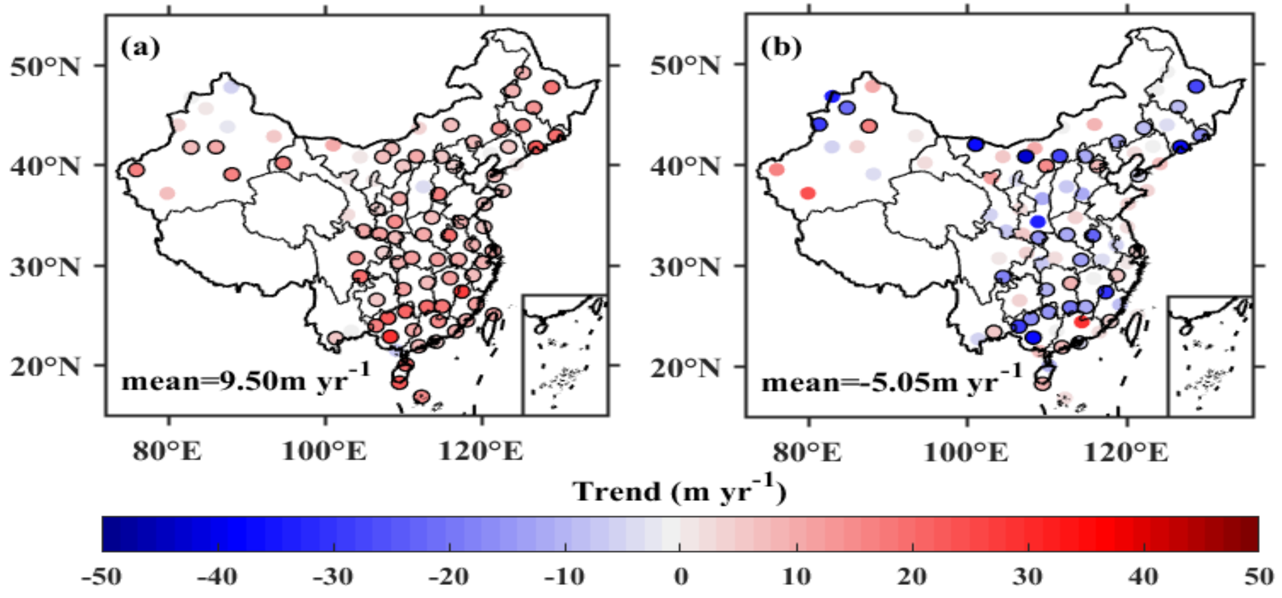


1979-2003

2004-2016

Spatial distr. of BLH trend over China

# Potential influential factors for the BLH trend shift

- Aerosol can not explain well the trend shift.
- Soil moisture dominates the trend shift of BLH during the period 1979 - 2016

1979-2003 2004-2016

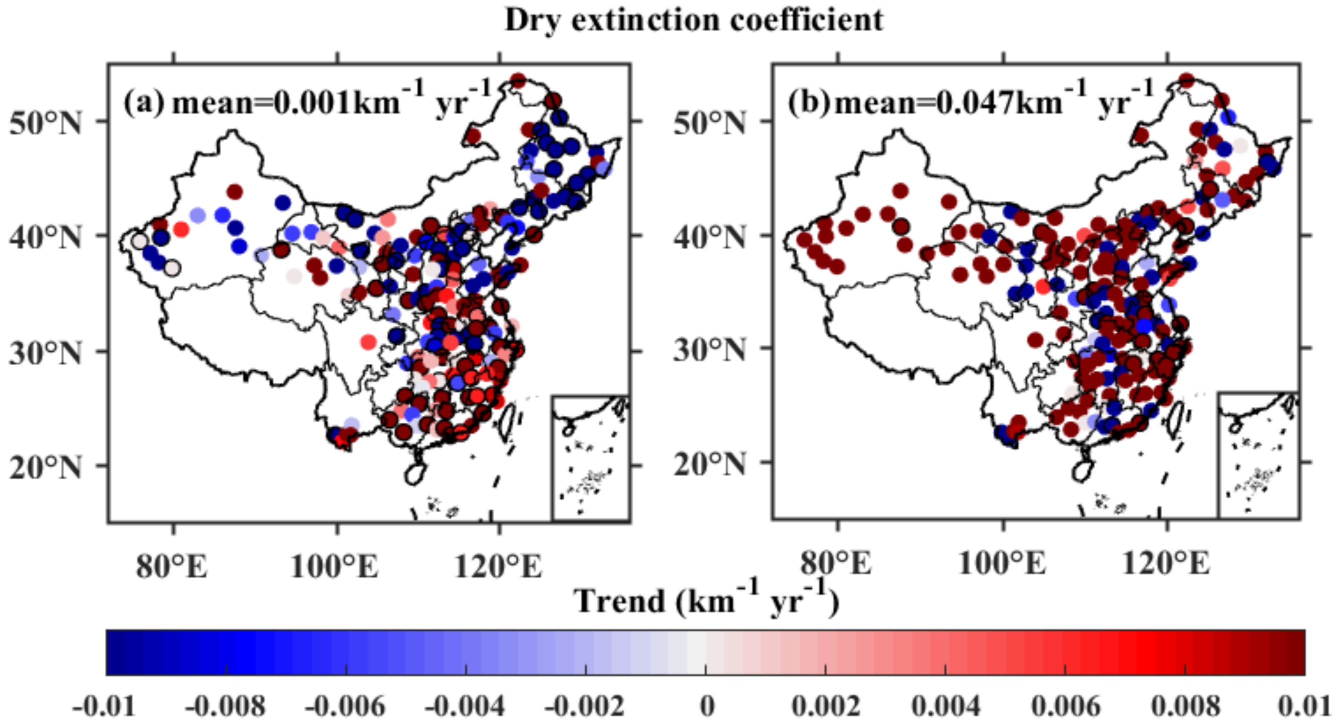


Dry extinction coefficient as derived from visibility was used as surrogate of aerosol loading.

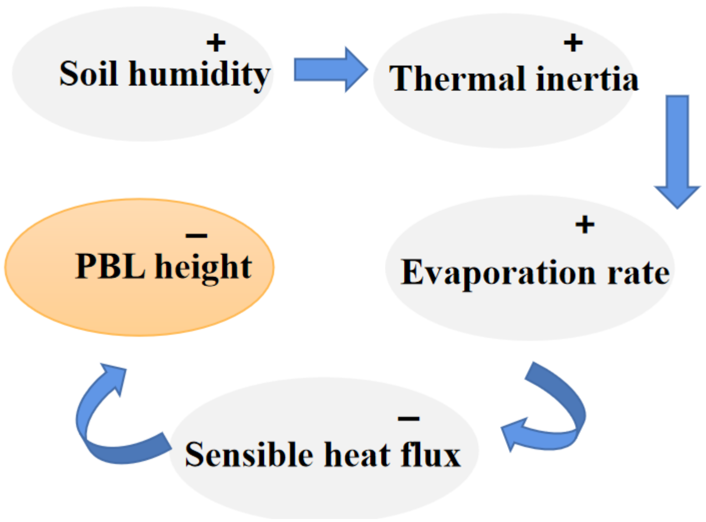


Schematic for the mechanism

Guo et al. GRL, 2019

# Trend of tropopause height in China from radiosondes

## 1979–2016 **In the background of global climate warming:**

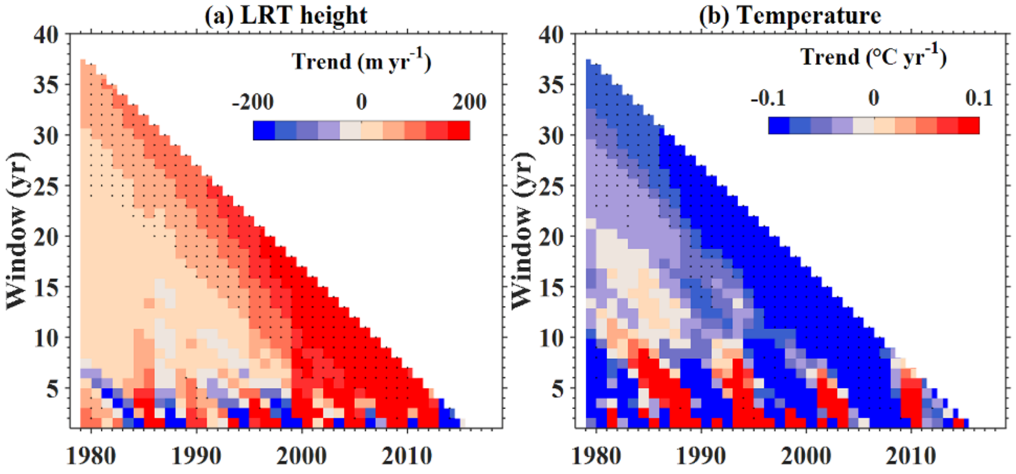


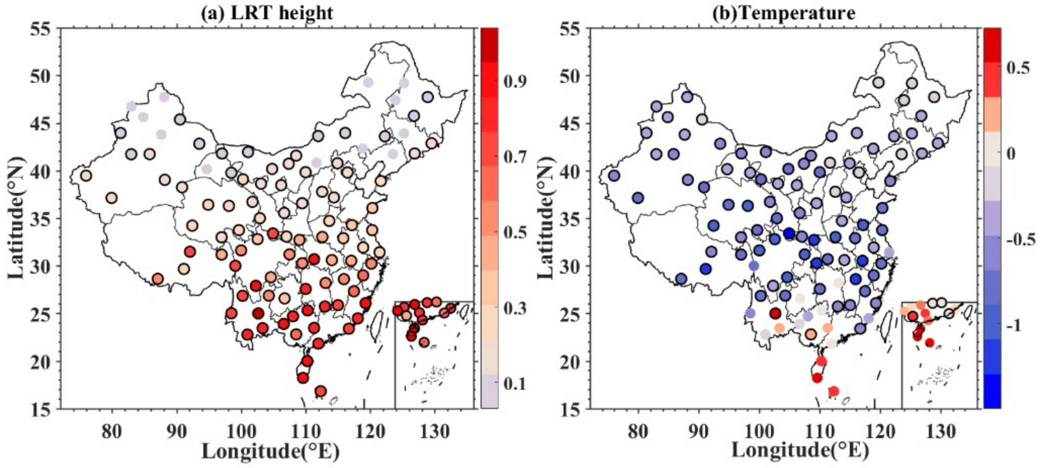


- The trend of lapse rate tropopause (LRT) height in most parts of China shows a significant upwards trend, with a five-year cycle of fluctuations.
- A clear seasonal variation, growth was fastest in August.

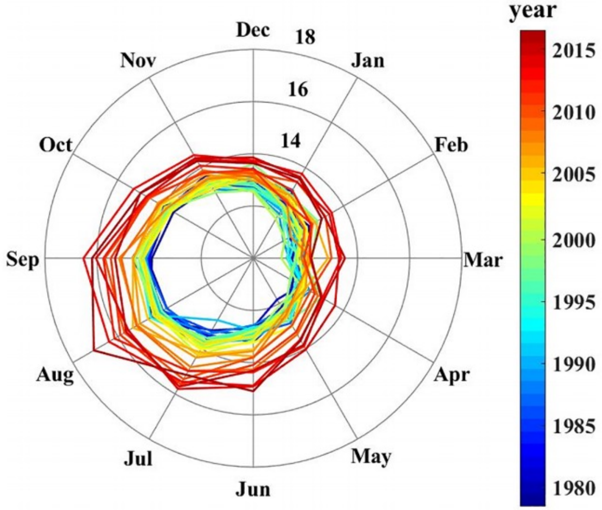


Chen et al., JOC 2019

# Trend of tropopause height in China from radiosondes

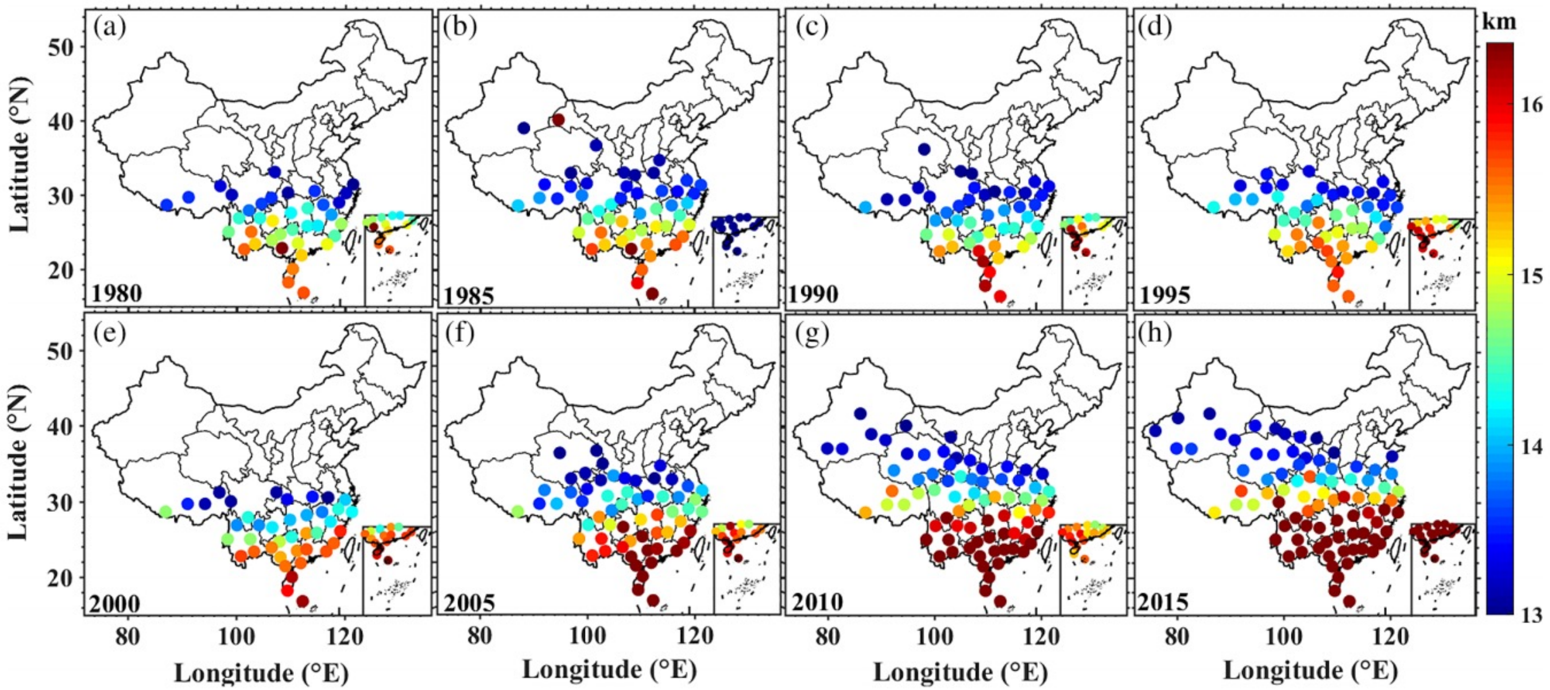


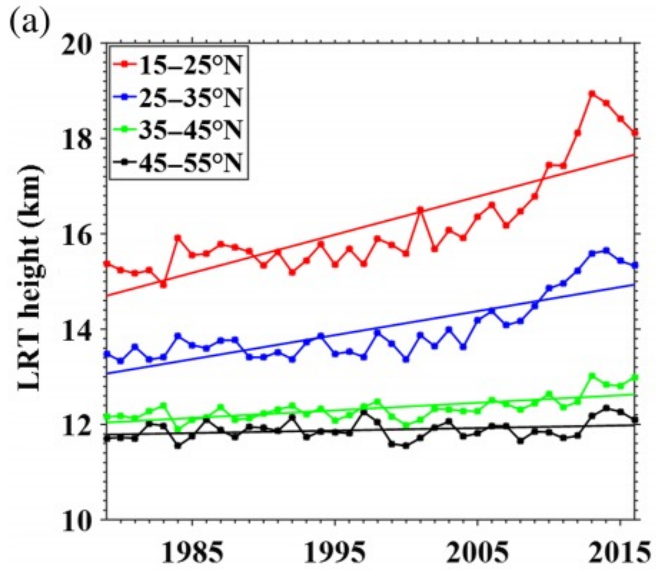


- The LRT height varies rapidly with latitudes, exhibiting a “south high and north low” pattern.
- LRT height over low latitudes is found to be expanding rapidly polewards.

Chen et al., JOC 2019

# Gravity waves (GW) derived from radiosondes

- **Gravity wave (GW) energy is extracted by the broad-spectral method. 2016-2019**
- **Seasonality of $E_t$ is dependent on latitudes, triggered by the shift in the winter subtropical jet.**

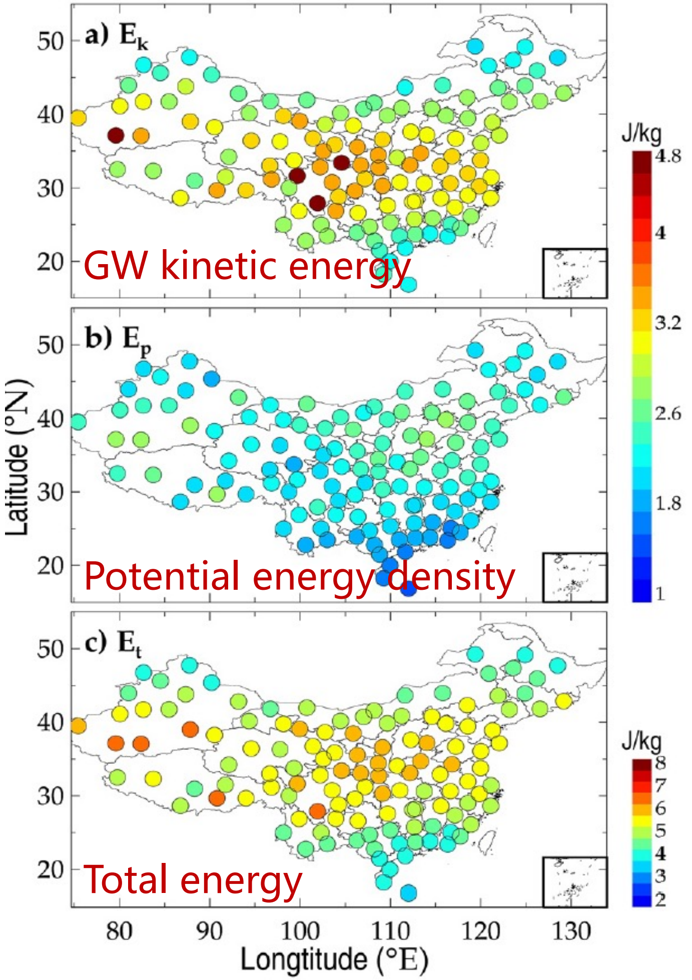


$$E_k = \frac{1}{2}\left[\overline{u'^2} + \overline{v'^2}\right]$$

$$E_p = \frac{1}{2}\frac{g^2\overline{\hat{T}'^2}}{N^2}$$

$$E_t = E_k + E_p$$

Highly correlated

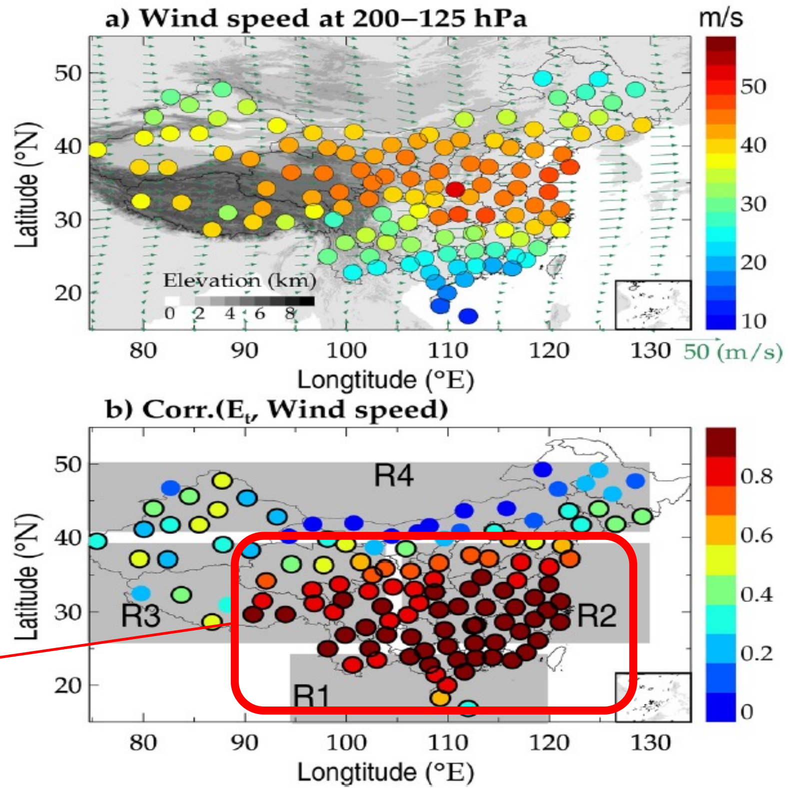


(Zhang et al., JGR, 2022)

# Potential sources for GW generation by random forests regressor

Kelvin-Helmholtz Instability

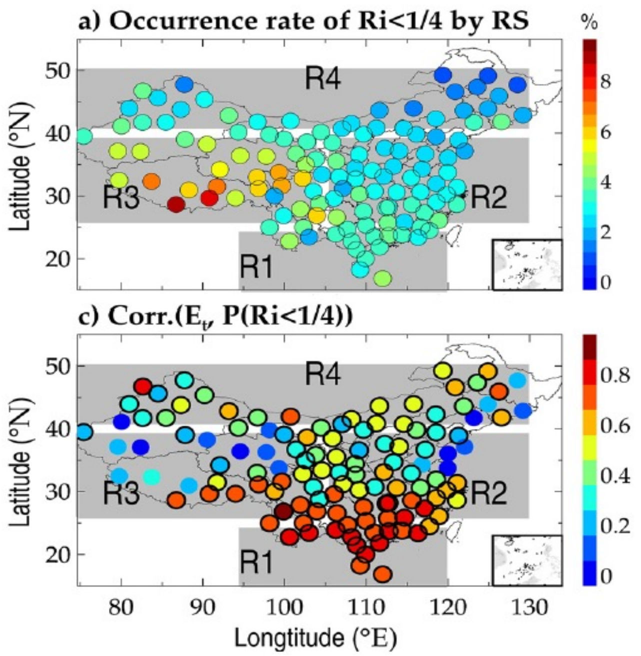


Terrain-induced flow

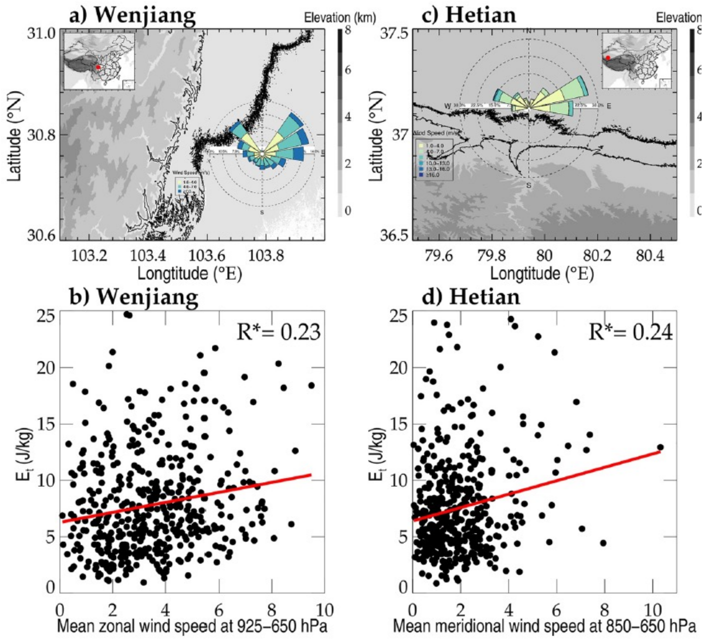


Precipitation

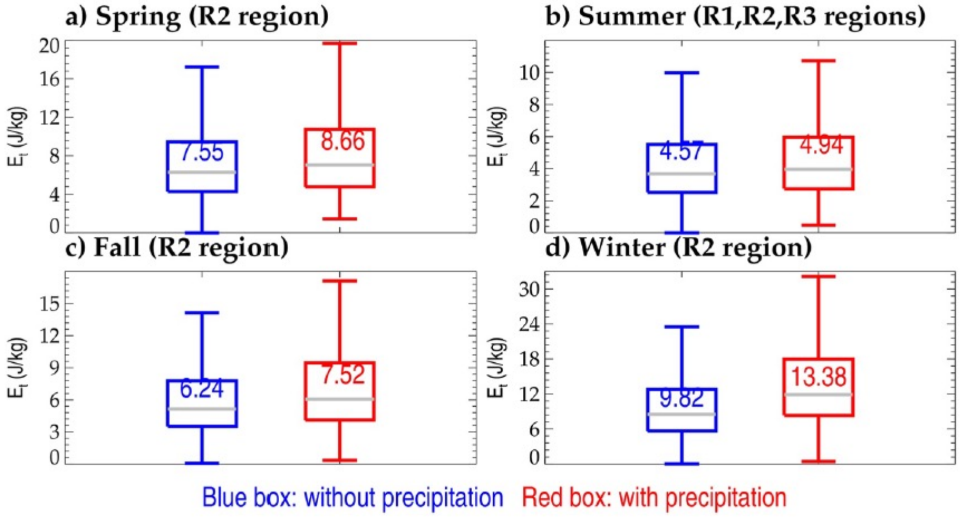


- In addition to the subtropical jet, **Kelvin-Helmholtz instability, terrain induced flow** and **precipitation** are also sources for GW generation.
- Except for northern China, the contribution to GW enhancement by convective precipitation is ~20% in summer.

(Zhang et al., JGR, 2022)

# Contributions to GW generation

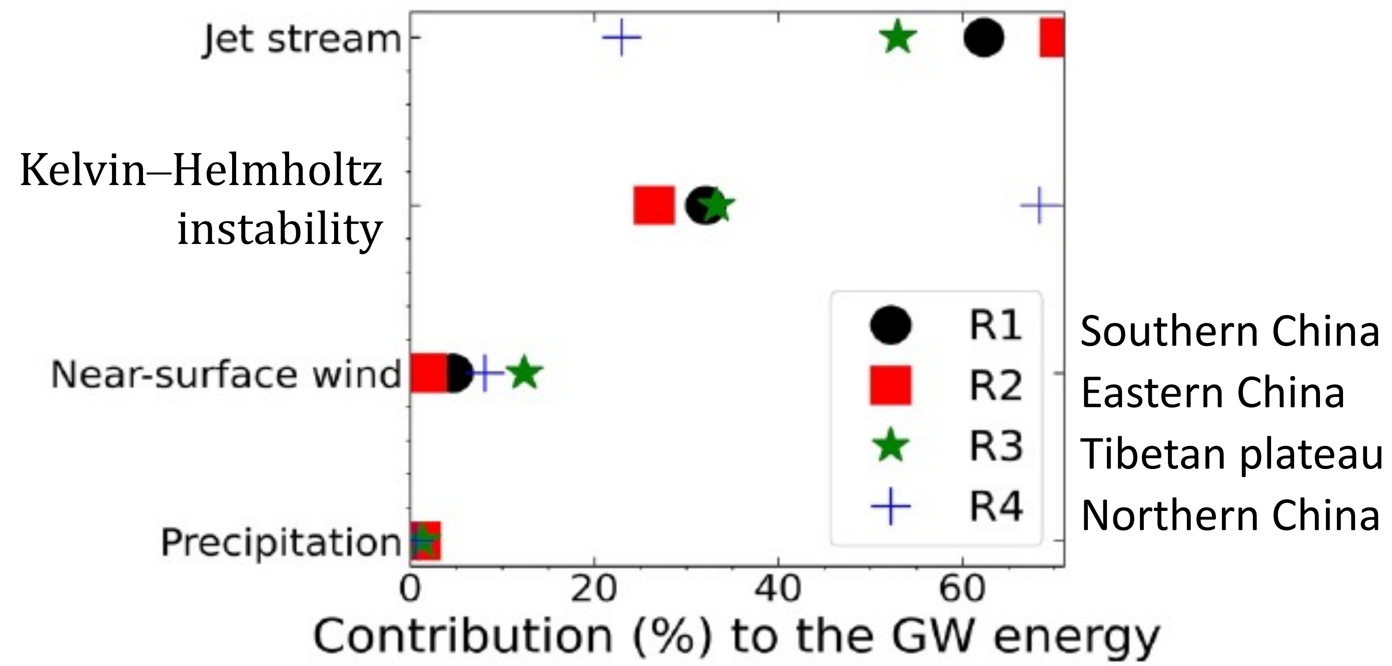


- **Jet stream is the dominant source for GWs.**
- **Enhanced GW activities favor large near-surface winds above Tibetan plateau.**
- **Considerably small contributions of precipitation is due largely to the low frequency of precipitation during nighttime sounding.**

(Zhang et al., JGR, 2022)

# Turbulence from radiosondes: features

- The turbulence dissipation rate(ε) was calculated using the Thorpe analysis. 2011–2018
- The clear-air ε in the free atmosphere with a 'south-high north-low'pattern.
- Large clear-air ε values were observed in both the LS and UT, especially over the Tibetan Plateau (TP).

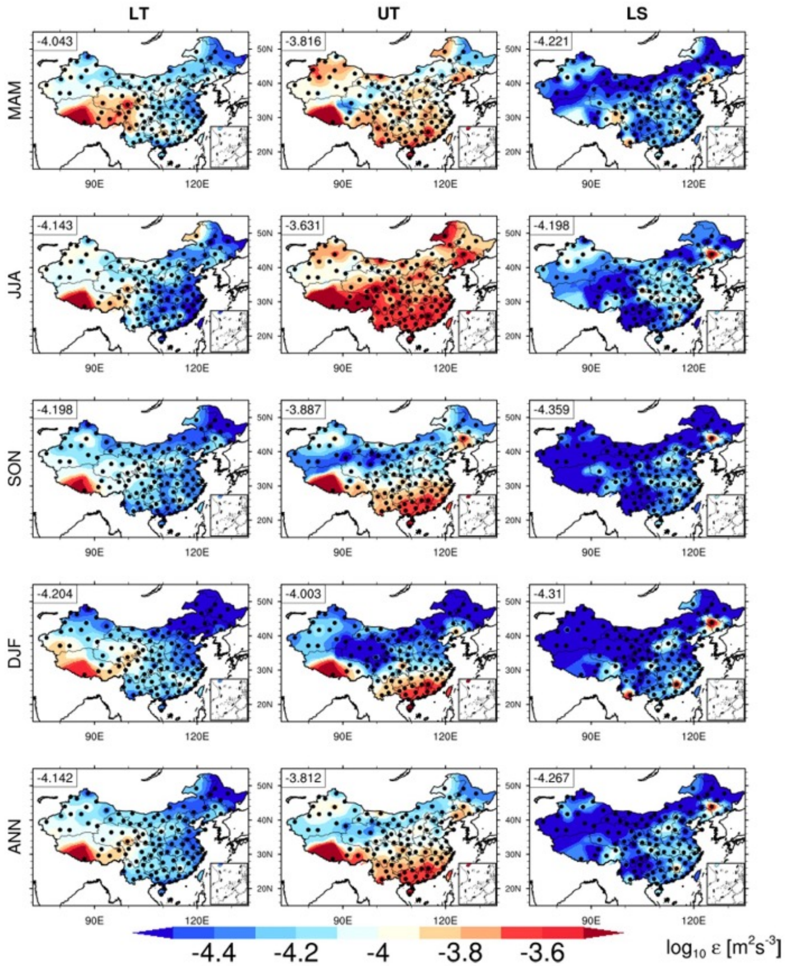


$$\varepsilon = C_K L_T^2 N^3$$

$$N = \sqrt{\frac{g}{\theta}\frac{d\theta}{dz}}$$

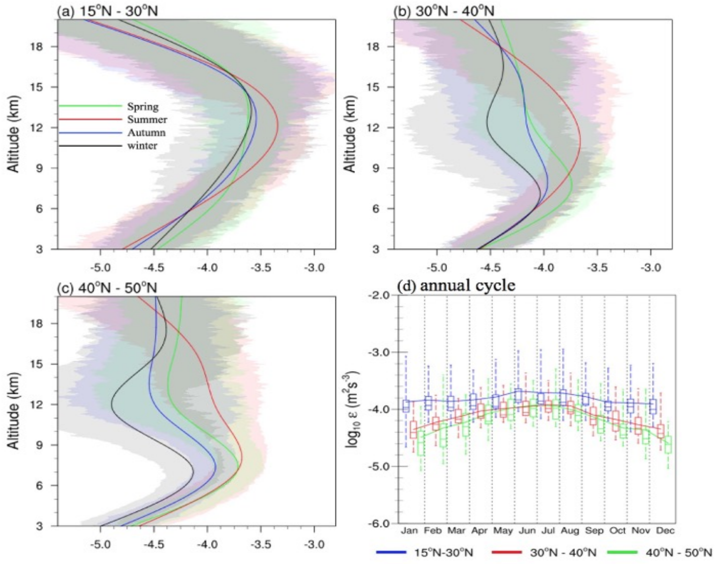


- The seasonality of ε was also pronounced, reaching maxima in summer and minima in winter.

Yanmin Lv et al Environ. Res. Let. 2021

# Turbulence from radiosondes: influential factors

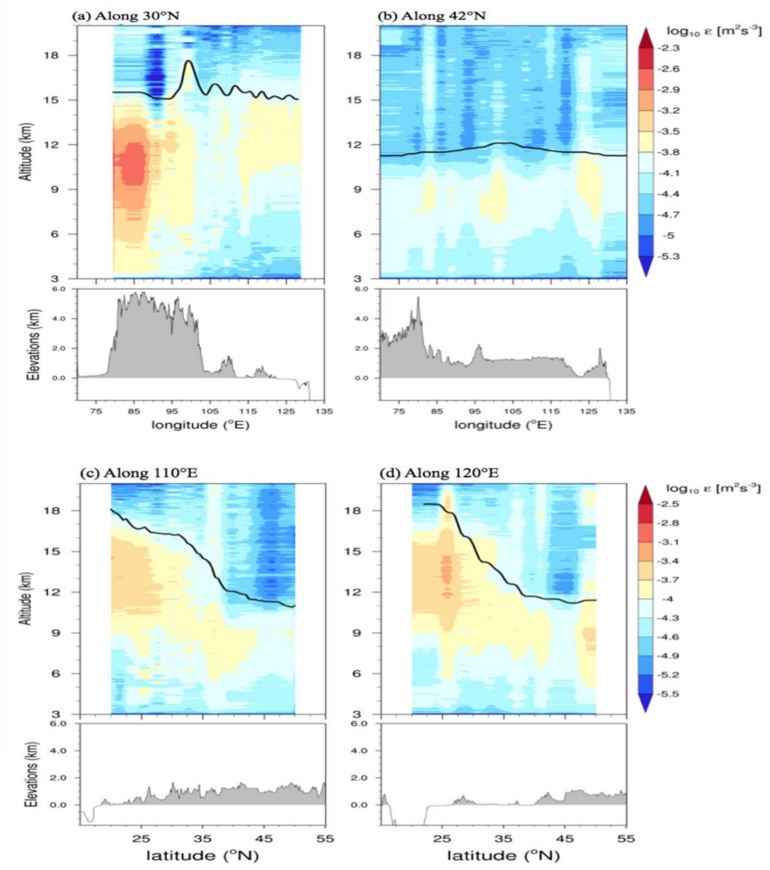


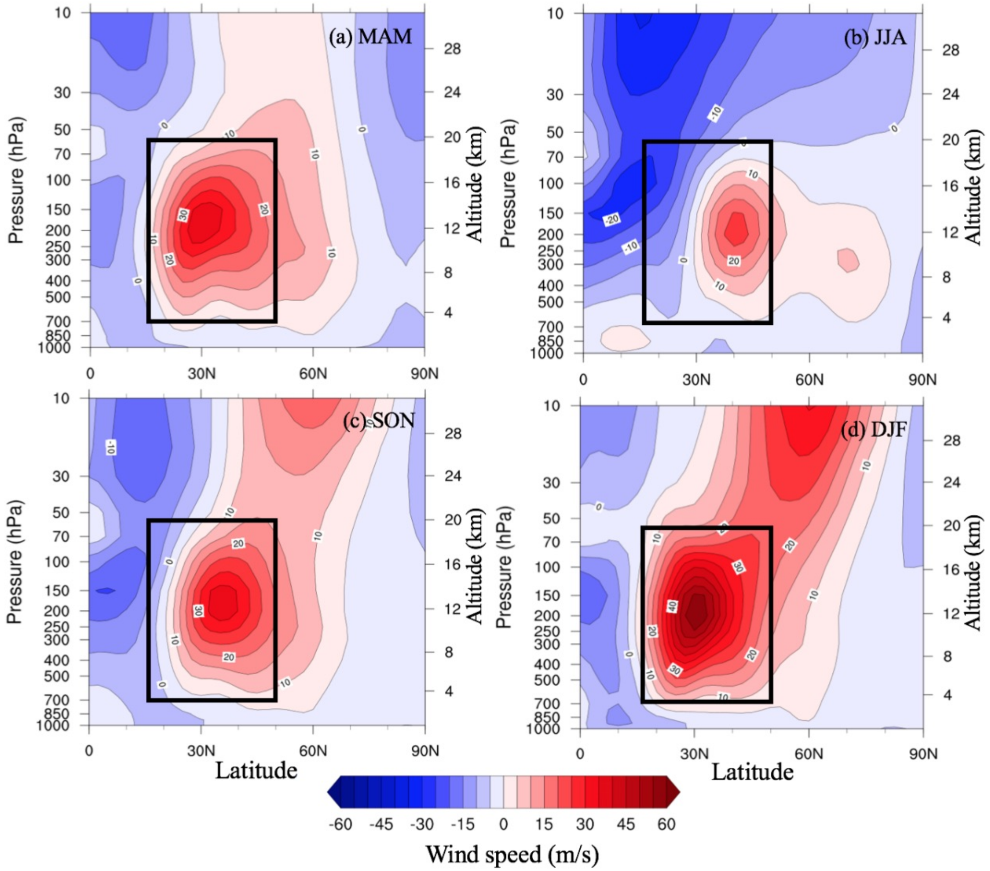


- Areas with large undulations in the terrain have strong turbulence.
- In the vertical direction, the altitude of peak clear-air ε in the troposphere was found to decrease poleward.
- Strong shear instability around westerly jet streams is an important source of turbulence.

Yanmin Lv et al Environ. Res. Let. 2021

# Beijing Mesosphere-Stratosphere-Troposphere (MST) radar

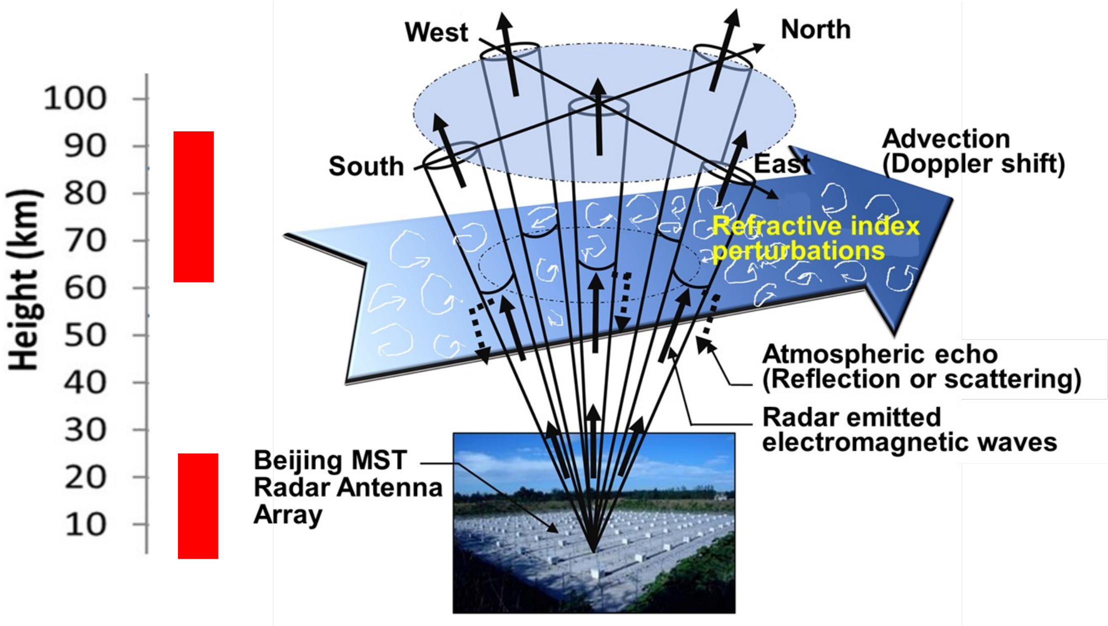



**2011 100m×100m**

**Provide continuous high time-height resolutions and quasi-simultaneous observations of the horizontal wind and vertical velocities of different height ranges.**

**Powerful tool for investigating various atmospheric dynamics (mean flow, tides, planetary waves, gravity waves, turbulence et al.) in the lower, middle and upper atmosphere.**

# Methods used to estimate turbulence parameters

$$\sigma^2_{tur} = \sigma^2_{obv} - \left(\sigma^2_{shear} + \sigma^2_{beam}\right)$$

$\sigma^2_{shear} + \sigma^2_{beam}$ $\begin{cases} \text{Horizontal wind} \\ \text{Vertical shear} \end{cases}$

$\sigma^2_{tur} < 0$:
**Negative turbulent kinetic energy (N-TKE).**

**Estimation models of $\sigma^2_{shear} + \sigma^2_{beam}$**

**H model** Hocking (1983,1985)

$$\sigma_{vb} = \sigma_{f\frac{1}{2}b} \cdot \frac{\lambda}{2}/(\sqrt{2ln2}) = (1.0) * 2/\lambda\theta_{1/2}V \cdot \frac{\lambda}{2}/\sqrt{2\ln 2} = (1.0) * \theta_{1/2}V/\sqrt{2\ln 2}$$

$$\sigma_{vs} = \sigma_{v\frac{1}{2}s}/(\sqrt{2ln2}) = \frac{1}{2} \cdot \left|\frac{\partial u}{\partial z}\right| \sin(\chi)\Delta r/(\sqrt{2ln2})$$

**N-2D model** Nastrom (1997)

$$\sigma^2_{shear+beam} = \frac{\theta^2}{3} v^2 cos^2\chi - \frac{2\theta^2}{3} sin^2\chi \left(v \frac{\partial v}{\partial z} rcos\chi\right)$$
$$+ \frac{\theta^2}{24}(3 + cos4\chi - 4cos2\chi)\left(\frac{\partial v}{\partial z}\right)^2 r^2 + \left(\frac{\theta^2}{3} cos4\chi + sin^2\chi cos^2\chi\right)\left(\frac{\partial v}{\partial z}\right)^2 \frac{\Delta r^2}{12}$$

**D-H model** Dehghan and Hocking (2011)

$$\sigma^2_{shear+beam} = \frac{\theta^2}{k} v^2 cos^2\chi - a_0 \frac{\theta}{k} sin\chi \left(v \frac{\partial v}{\partial z}\zeta\right) + b_0 \frac{2sin^2\chi}{8k}\left(\frac{\partial v}{\partial z}\zeta\right)^2$$
$$+ c_0(sin^2\chi cos^2\chi)|v\xi| + d_0(sin^2\chi cos^2\chi)\xi^2$$

**The turbulent kinetic energy dissipation rate** $\varepsilon = A^{-3/2} N \sigma^2_{tur}$

**The vertical eddy diffusion coefficient** $K_z = 0.15 N^{-1} \sigma^2_{tur}$

# The applicability of three models in different wind field conditions

**Data： Beijing MST radar 2012-2014 37 000 profiles**

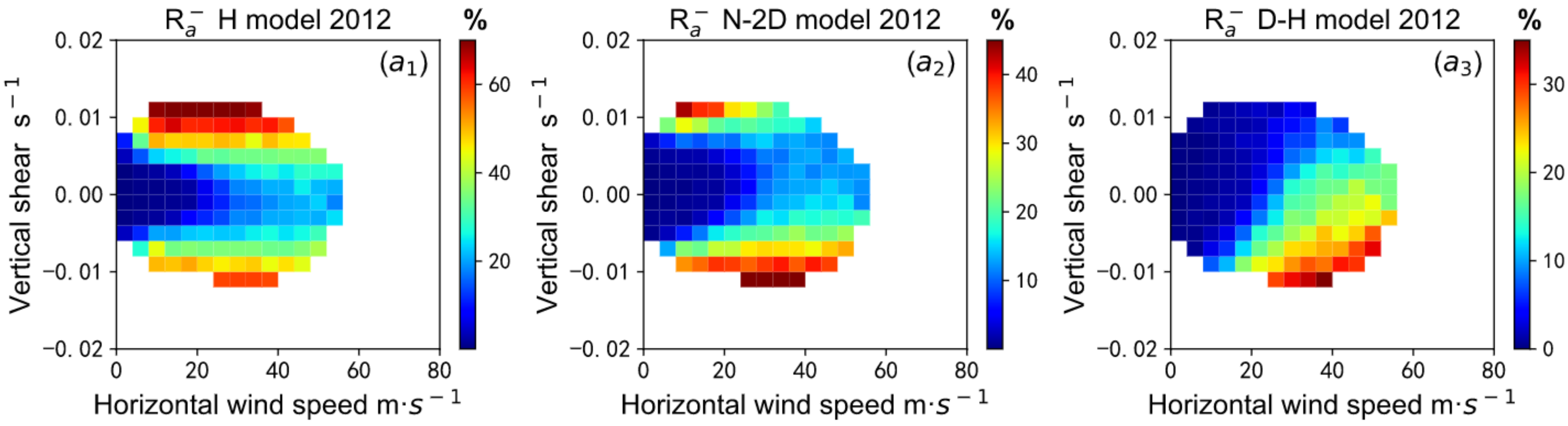


**The proportion of N-TKE in the H model, N-2D model and D-H model increases with the horizontal wind speed and the vertical shear of horizontal wind speed.**

**The maximum values are 80 %, 45 % and 35 %, respectively.**

# The applicability of three models in different wind field conditions

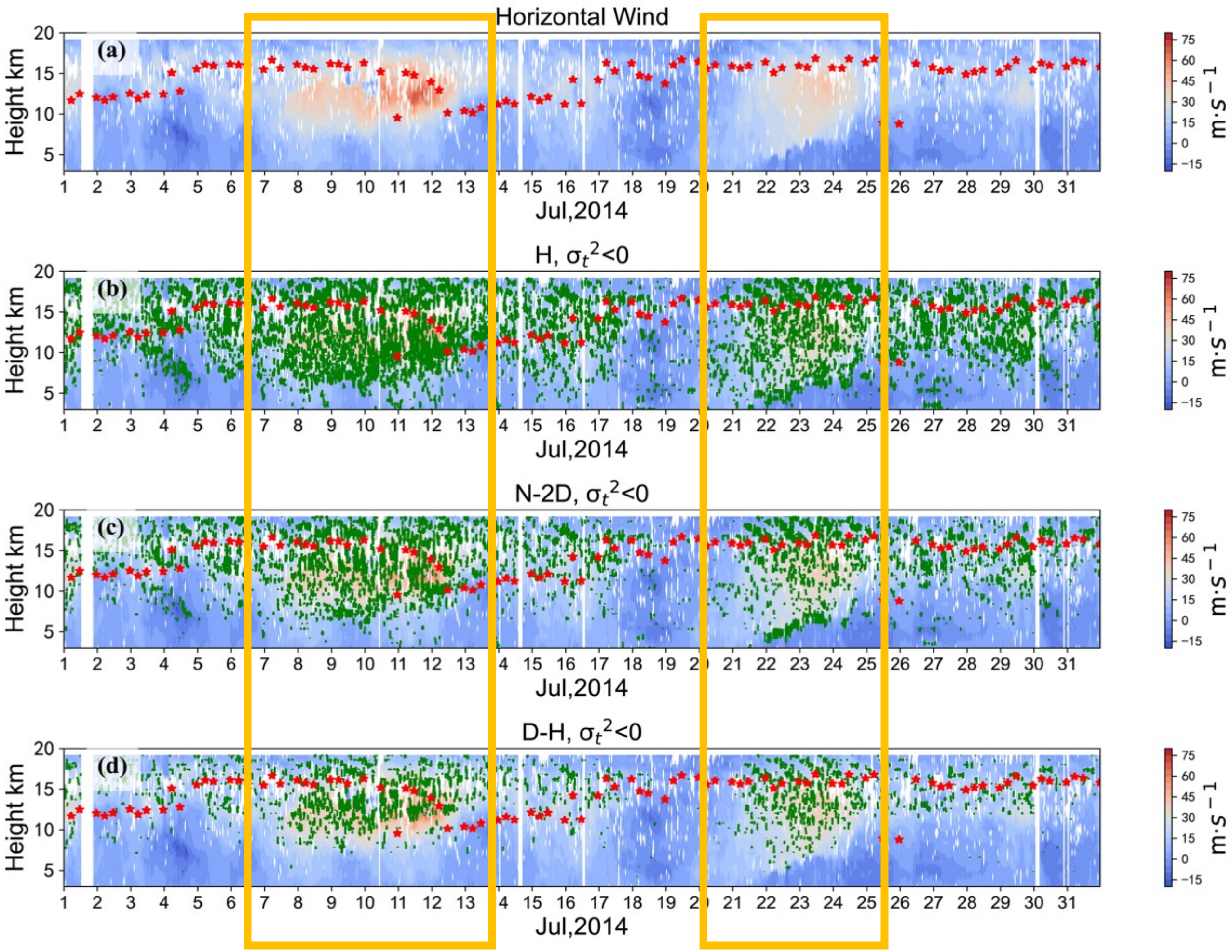


**Green: N-TKE**

**Red: Tropopause height**

**Orange: Strong wind period**

**It is still necessary to consider the applicability of the N-2D model and D–H model in some weather processes with strong winds.**

# Distribution characteristics of the turbulence parameters in the troposphere-lower stratosphere

### The turbulent kinetic energy dissipation rate

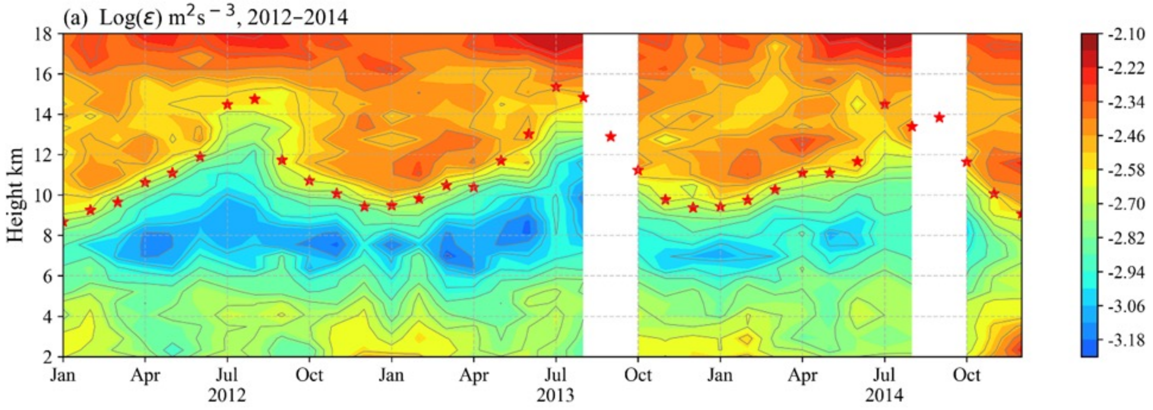


### The vertical eddy diffusion coefficient

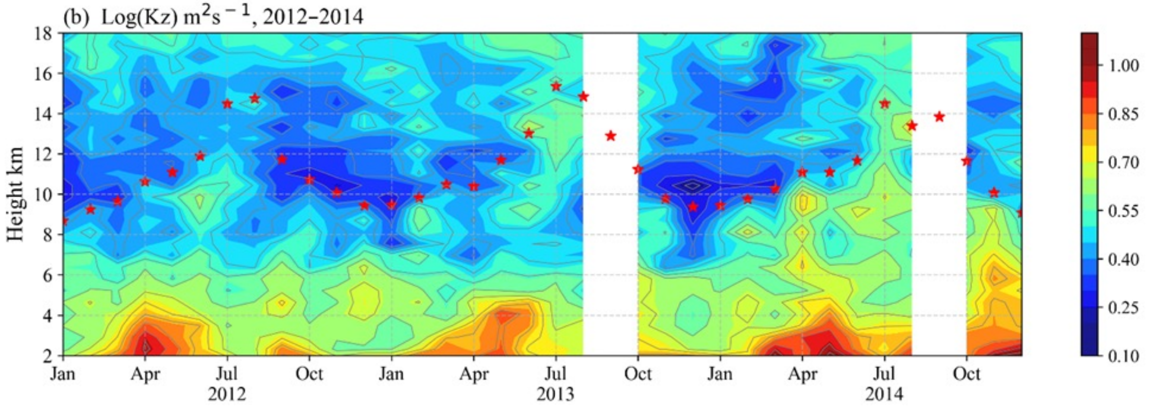


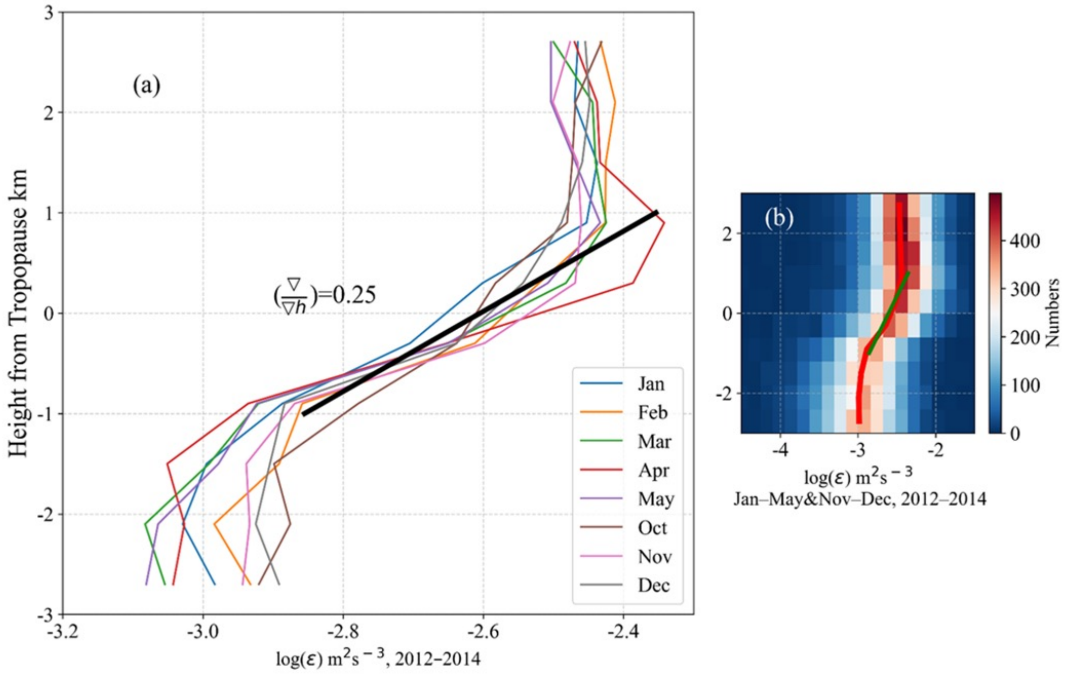


**The seasonal variation of turbulence parameters has noticeable differences at different atmospheric layers.**

# The atmospheric static/dynamic stability and turbulence intensity influence the distribution of the turbulence parameters

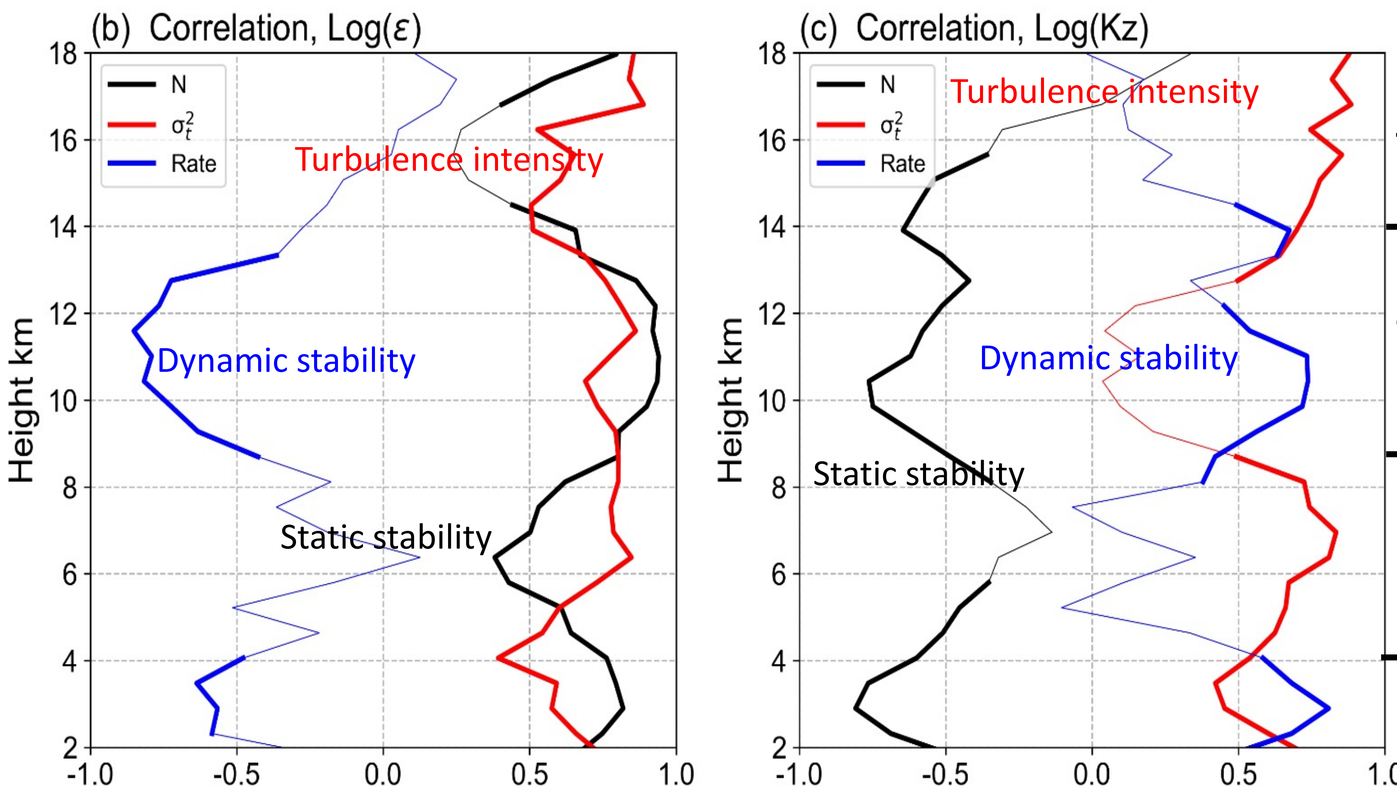


14~18 km： Turbulence intensity

9~14 km

$\boldsymbol{\varepsilon}$ stability, turbulence intensity

$\boldsymbol{K_z}$ stability

4~9 km： Turbulence intensity

2~4 km： Static/dynamic stability

# Related papers


Guo, J. P., Y. C. Miao, Y. Zhang, H. Liu, Z. Q. Li, W. C. Zhang, J. He, et al. "The Climatology of Planetary Boundary Layer Height in China Derived from Radiosonde and Reanalysis Data." Atmospheric Chemistry and Physics 16, no. 20 (Oct 2016): 13309-19. https://doi.org/10.5194/acp-16-13309-2016.

Zhang, Wanchun, Jianping Guo, Yucong Miao, Huan Liu, Yu Song, Zhang Fang, Jing He, et al. "On the Summertime Planetary Boundary Layer with Different Thermodynamic Stability in China: A Radiosonde Perspective." Journal of Climate 31, no. 4 (Feb 2018): 1451-65. https://doi.org/10.1175/jcli-d-17-0231.1.

Guo, J., Li, Y., Cohen, J. B., Li, J., Chen, D., Xu, H., et al. (2019). Shift in the temporal trend of boundary layer height in China using long-term (1979–2016) radiosonde data. Geophysical Research Letters, 46, 6080–6089. https://doi.org/10.1029/ 2019GL082666

Chen, Xinyan, Jianping Guo, Jinfang Yin, Yong Zhang, Yucong Miao, Yuxing Yun, Lin Liu, et al. "Tropopause Trend across China from 1979 to 2016: A Revisit with Updated Radiosonde Measurements." International Journal of Climatology 39, no. 2 (Feb 2019): 1117-27. https://doi.org/10.1002/joc.5866.

Zhang, J., Guo, J.*, Xue, H., Zhang, S., Huang, K., Dong, W., et al. (2022). Tropospheric gravity waves as observed by the high-resolution China Radiosonde Network and their potential sources. Journal of Geophysical Research: Atmospheres, 127, e2022JD037174. https://doi.org/10.1029/2022JD037174

Lv, Yanmin, Jianping Guo, Jian Li, Lijuan Cao, Tianmeng Chen, Ding Wang, Dandan Chen, et al. "Spatiotemporal Characteristics of Atmospheric Turbulence over China Estimated Using Operational High-Resolution Soundings." Environmental Research Letters 16, no. 5 (May 2021). https://doi.org/10.1088/1748-9326/abf461.

Chen, Z.; Tian, Yufang*; Lü, D. Turbulence Parameters in the Troposphere—Lower Stratosphere Observed by Beijing MST Radar. Remote Sens. 2022, 14, 947. https:// doi.org/10.3390/rs14040947

Chen, Z., Tian, Yufang*., Wang, Y., Bi, Y., Wu, X., Huo, J., Pan, L., Wang, Y., and Lü, D.: Turbulence parameters measured by the Beijing mesosphere–stratosphere-troposphere radar in the troposphere and lower stratosphere with three models: comparison and analyses, Atmos. Meas. Tech., 15, 4785–4800, https://doi.org/10.5194/amt-15-4785-2022, 2022.

# Thank you very much for your attention!

Jianping Guo (jpguocams@gmail.com)
Yufang Tian (tianyufang@mail.iap.ac.cn)